Structure, Vol. 12, 1281–1288, July, 2004, ©2004 Elsevier Ltd. All rights reserved. DOI 10.1016/j.str.2004.04.016

Mechanism of Primary Proton Transfer in Bacteriorhodopsin

Ana-Nicoleta Bondar,[1,2] Marcus Elstner,[2,3] Sándor Suhai,[2] Jeremy C. Smith,[1] and Stefan Fischer[1,*]

[1]Computational Molecular Biophysics
IWR
Heidelberg University
Im Neuenheimer Feld 368
Heidelberg
Germany

[2]Molecular Biophysics Department
German Cancer Research Center
Im Neuenheimer Feld 580
D-69120 Heidelberg
Germany

[3]Theoretische Physik
University of Paderborn
Warburger Strasse 100
33098 Paderborn
Germany

Summary

Recent structures of putative intermediates in the bacteriorhodopsin photocycle have provided valuable snapshots of the mechanism by which protons are pumped across the membrane. However, key steps remain highly controversial, particularly the proton transfer occurring immediately after retinal *trans*→*cis* photoisomerization. The gradual release of stored energy is inherently nonequilibrium: which photocycle intermediates are populated depends not only on their energy but also on their interconversion rates. To understand why the photocycle follows a productive (i.e., pumping), rather than some unproductive, relaxation pathway, it is necessary to know the relative energy barriers of individual steps. To discriminate between the many proposed scenarios of this process, we computed all its possible minimum-energy paths. This reveals that not one, but three very different pathways have energy barriers consistent with experiment. This result reconciles the conflicting views held on the mechanism and suggests a strategy by which the protein renders this essential step resilient.

Introduction

Bacteriorhodopsin is a seven-helical light-driven proton pump protein found in the purple membrane of the archea *Halobacterium salinarium* (Figure 1A). The absorption of one photon by the all-*trans* retinal chromophore leads to rotation of the C13=C14 bond into the 13-*cis* conformation (Figure 1B). This triggers a photocycle through a series of intermediates distinguished spectroscopically:

$$bR_{568} \rightarrow J_{625} \rightarrow K_{590} \rightarrow L_{550} \rightarrow M_{412} \rightarrow N_{620} \rightarrow O_{640} \rightarrow bR_{568}$$

The net effect is the transfer of one proton from the cytoplasmic to the extracellular side of the membrane (recently reviewed in Subramaniam et al., 1999; Lanyi, 2000; Neutze et al., 2002). The resulting electrochemical gradient is used by the cell to synthesize adenosine triphosphate (ATP). The first proton transfer occurs between the L and M states on a time scale of ~10 μs (Ludman et al., 1998). In this key step, a proton is transferred from the retinal Schiff base to Asp85. The mechanism of this primary step is still under much debate (Lanyi 2000; Neutze et al., 2002). Available crystal structures suggest different orientations of the Schiff base NH group (Figure 1B), leading to controversy as to how 13-*cis* retinal is twisted before deprotonation. This is essential because it determines the transfer mechanism, and also because it has been proposed that retinal untwisting upon deprotonation triggers the conformational changes required by subsequent vectorial transport (Lanyi and Schobert, 2003). Another question is how can the proton be transferred over the ~4 Å distance, which is too long for a direct jump. Various alternatives have been proposed, involving proton wires via intermediate proton carriers, either on the Thr89 (Subramaniam and Henderson, 2000; Edman et al., 2003) or on the Asp212 (Lanyi and Schobert, 2003) side of the retinal (Figure 1C). A proton wire allows transfer over larger distances because the proton given by the Schiff base is not the same proton accepted by Asp85. This is illustrated as follows for the case of a single intermediate carrier (I):

$$\text{SB-H1} \cdots \text{I-H2} \cdots \text{Asp85} \rightarrow \text{SB} \cdots \text{H1-I} \cdots \text{H2-Asp85}.$$

The need to use theoretical methods to address these intertwined questions has been stressed again recently (Edman et al., 2003). Indeed, the gradual release of stored energy to drive vectorial proton transfer is inherently nonequilibrium. Although there exist numerous high-resolution X-ray crystallographic and electron microscopic structures of bacteriorhodopsin and its putative photocycle intermediates (Belrhali et al., 1999; Luecke et al., 1999; Edman et al., 1999; Royant et al., 2000; Sass et al., 2000; Subramaniam and Henderson 2000; Schobert et al., 2002; Lanyi and Schobert, 2002, 2003), trapping and assigning the relevant intermediates is difficult. From the simulation point of view, this means that transient states are populated not only based on their relative energy but also on their interconversion rates. Therefore, to understand why the photocyle follows some pathways and not others, it is necessary to know the energy barrier of the proton transfer paths.

Here, the different mechanisms of the primary proton transfer were exhaustively explored by computing minimum-energy paths for more than 40 transfer scenarios, varying elements such as the number and location of nearby water molecules, the initial orientation of the Schiff base, the intermediate proton acceptors involved,

*Correspondence: stefan.fischer@iwr.uni-heidelberg.de

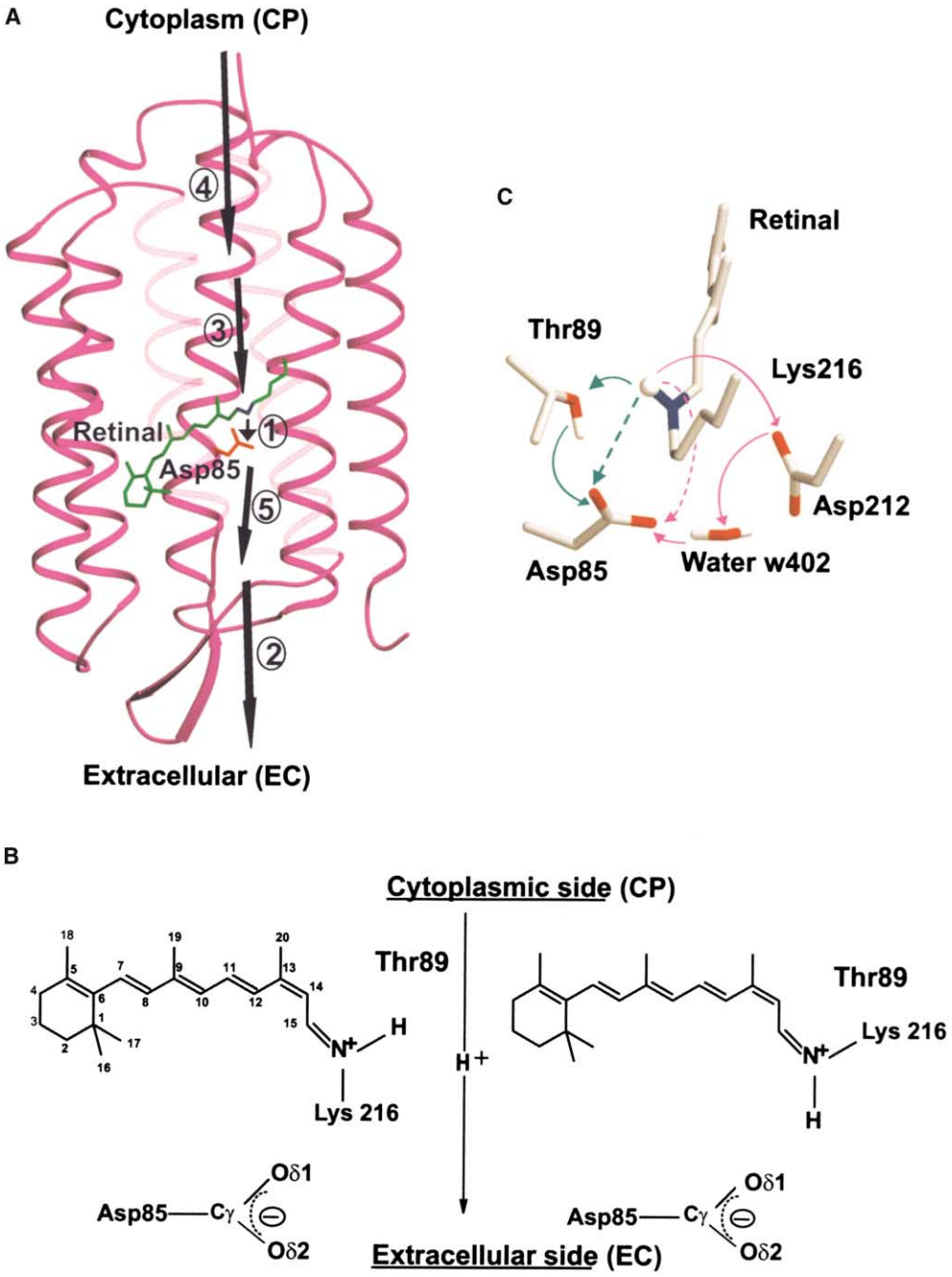

Figure 1. The Primary Proton-Transfer Step

(A) Order of proton transfer steps in the photocycle. (1) Primary proton transfer from the Schiff-base NH to Asp85. (2) Proton release to the extracellular side. (3) Reprotonation of the Schiff base from Asp96 (followed by thermal back-isomerization of retinal). (4) Reprotonation of Asp96 from the cytoplasmic side. (5) Protonation of the extracellular release-group from Asp85.

(B) Putative orientations of the Schiff-base proton before primary transfer: left, toward the cytoplasm and away from Asp85 (the C15=N bond is 15-*anti*); right, toward the extracellular side (shown here in 15-*syn*, this orientation can also be achieved by a twisted 15-*anti* or a 13,14-*dicis* configuration).

(C) The primary transfer could be on either side of retinal (green or magenta arrows) and could be either direct (broken lines) or via intermediate proton carriers (continuous lines).

and with different protein crystal structures. The calculations yield atomic-detail movies (available under http://www.iwr.uni-heidelberg.de/groups/biocomp/fischer) of the most probable transfer pathways, which can be distinguished on the basis of their rate-limiting energy barriers. Potential energy barriers are meaningful here because it has been found that enthalpy dominates the free-energy barrier of the primary proton transfer (Lud-

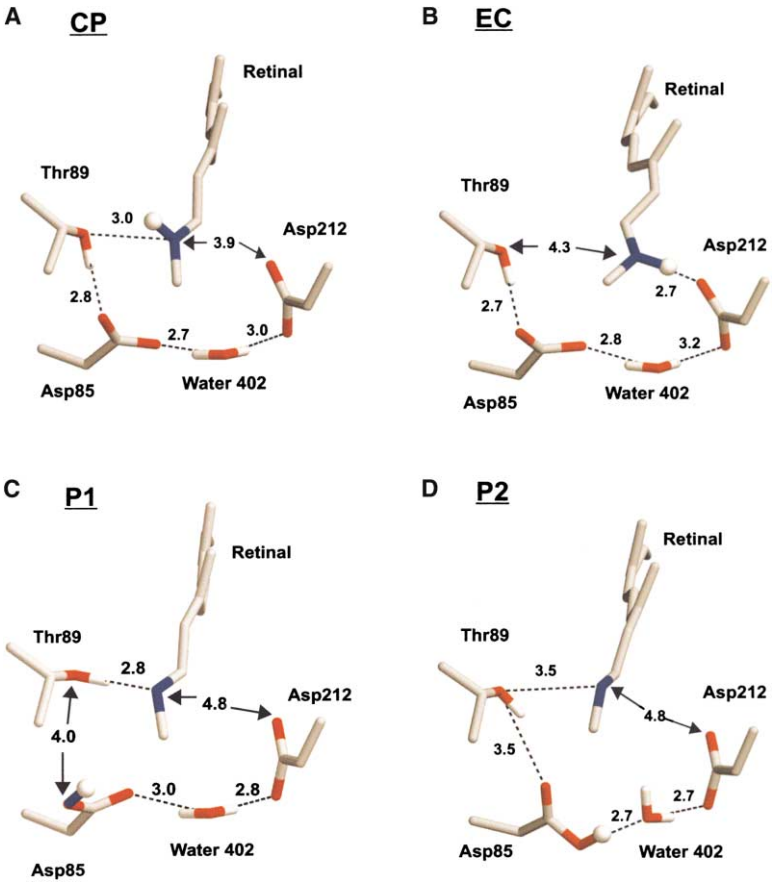

Figure 2. End States of Primary Proton Transfer

(A and B) Energy-optimized reactant structures with the Schiff-base twisted toward (A) the cytoplasmic side (CP), or (B) toward the extracellular side (EC).

(C and D) Product structures with different orientations of the protonated Asp85 side chain (P1, P2). Hydrogen bonds (dotted lines) distances (in angstroms) are between heavy atoms, other distances shown with arrows.

man et al., 1998). Combining the knowledge of the different energy barriers with the experimental conversion rates leads to two unexpected conclusions: (1) Before transfer, the retinal accumulates in a conformation with the Schiff base NH group pointing in the direction opposite to proton pumping; and (2) three very different transfer mechanisms have energy barriers consistent with experiment.

Results

Initial State

First, we describe models for the "initial" and "final" states, which we define as those states accumulating immediately before and after the primary proton transfer. For the initial state, two energy-optimized conformations of 13-*cis*, 15-*anti* retinal were found to be stable. One of these has the Schiff base NH bond directed toward the cytoplasmic side (called here the "CP state," Figure 2A), and the other toward the extracellular side (called here the "EC state," Figure 2B). In both, the retinal polyene chain is twisted (i.e., nonplanar), but much more so for the EC than for the CP state. This energetically unfavorable twisting allows the positively charged Schiff base to make a hydrogen bond to Thr89 in the CP state and a salt bridge to Asp212 in the EC state. The geometry of the protein residues surrounding the retinal is closely similar in the CP and EC conformations. In particular, a hydrogen bond between Asp85 and Thr89 forms. This hydrogen bond is consistent with FTIR spectroscopic data that indicate its presence in the L state (Kandori et al., 2001).

The conformation of the Schiff base in the crystal structures available for the K and L states varies considerably (Edman et al., 1999; Royant et al., 2000, Schobert et al., 2002; Lanyi and Schobert, 2003; Edman et al., 2003), making it difficult to decide which of the EC and CP conformers is the "initial" state of proton transfer. Therefore, we discriminate here between these two conformers based on energetic considerations. The energy difference between the EC and CP conformations is significant, CP being 5.9 kcal/mol lower. However, due to the nonequilibrium nature of the early bR photocycle, knowledge of the energy difference is not sufficient to permit assignment of the CP state to the accumulating L_{550} spectroscopic intermediate. Indeed, we cannot exclude that earlier steps of the photocycle might produce the EC conformer at first. However, we can examine whether this state would be more likely to convert to the CP conformation or rather would prefer to initiate proton transfer. For this purpose, the minimum energy pathway between the CP and EC conformations was calculated. The resulting rate-limiting barrier for the EC-to-CP transition is 2.4 kcal/mol. This small energy barrier means that EC can convert to CP on the subnanosecond timescale. This is likely to occur, since the subsequent step (i.e., proton transfer) is known to happen much more slowly, on the microsecond time scale (Ludman

Table 1. Optimized Geometry of the Retinal after Primary Proton Transfer

	P1	P2	NMR[a,b]
H-C14-C15-H (°)[c]	−149.9	−161.8	±147 (±10)
C14···Cγ (Asp85) (Å)[d]	6.4	6.7	>6
C14···Cγ (Asp212) (Å)[d]	5.4	5.4	4.8 (±1.0)

[a] Griffiths et al. (2000).
[b] Lansing et al. (2002).
[c] Torsion angle of the C14-C15 bond of retinal.
[d] Distance between retinal C14 and the protein atom.

Table 2. Rate-Limiting Energy Barriers for Primary Proton Transfer

Pathway	Member of Proton Wire	Barrier (kcal/mol)[a]
1a	–	12.4
1b	–	27.8
2	Thr89	13.6
3a	Asp212[b], water w402	11.5
3b[c]	Asp212[b], water w402	16.7
4a	water w402	17.5
4b[c]	water w402	14.1
5[d]	–	12.3

[a] Barriers are relative to the "initial" CP state (Figure 2A).
[b] Asp212 acts as a transient proton acceptor.
[c] Paths going through the 13,14-*dicis* retinal configuration.
[d] Thr89Val mutant.

et al., 1998). Once the protein is in the CP conformation, conversion back to EC has a high barrier of 8.2 kcal/mol. In contrast, path calculations detailed below show that the barrier for proton transfer from the EC state is 5.7 kcal/mol. This barrier is twice as high as for the conformational conversion to CP. This means that the EC state can be populated transiently, but most often prefers to revert back to CP than to proceed with proton transfer. Furthermore, this barrier is too low to account for the experimental time scale of proton transfer. The barrier for proton transfer from the CP state is found to be 11–13 kcal/mol (see below), consistent with the experimental microsecond time scale. The ensemble of the above results leads to the proposal that the state accumulating before proton transfer is in a CP conformation (Figure 2A). Therefore, the primary proton transfer pathways will be discussed here starting from the CP state, which is used as reference to determine the corresponding rate-limiting energy barriers.

Final State

After transfer, the proton resides on one of the acidic oxygens of Asp85. The respective structures are called here P1 (Figure 2C) and P2 (Figure 2D). Both P1 and P2 are consistent with experimental data for the M state: FTIR data suggesting that Thr89 makes a hydrogen bond (Kandori et al., 2001), nuclear magnetic resonance (NMR) data indicating that the deprotonated Schiff base is hydrogen bonded (Hu et al., 1998), and NMR data (Griffiths et al., 2000; Lansing et al., 2002) on the active site geometry (see Table 1). We find that P1 is 3.8 kcal/mol higher than P2. Mechanisms that were considered for the conversion of P1 to P2 are the rotation of the Asp85 side chain or the proton transfer from oxygen atom $O_{\delta 1}$ to $O_{\delta 2}$. Minimum energy paths were computed for both these possibilities. The proton transfer path was found to have a 31.5 kcal/mol activation barrier and is therefore highly unlikely. In contrast, the rotation mechanism has a barrier of only 4.4 kcal/mol, such that P1 can convert into P2 on the subnanosecond timescale. The P1 state is 0.8 kcal/mol above, whereas P2 is 3 kcal/mol below the CP state. This is consistent with the experimental data showing that the product and reactant states should be approximately isoenergetic (Ludman et al., 1998).

These post proton-transfer states have retinal twisted toward Thr89, like the pretransfer CP state. Thus, the protein conformational changes subsequent to deprotonation are unlikely to be triggered by retinal untwisting, but rather by a displacement of the Schiff base toward the cytoplasm, as previously suggested (Subramaniam and Henderson, 2000). This displacement is observed here and is accompanied by a motion of Asp85 in the opposite direction (Figures 2A and 2C).

Proton Transfer Pathways

Several mechanisms are conceivable for primary proton transfer (Figure 1C). First, the transfer could take place on either sides of the retinal plane: the Thr89 side or the Asp212 side. Second, the transfer could be either direct or involve intermediate proton carriers: on the Thr89 side via a proton wire with Thr89, and on the Asp212 side via transient protonation of Asp212 and/or a proton wire with water molecule w402. For all these scenarios, minimum energy pathways and their rate-limiting energy barriers were computed. Additionally, since several crystal structures have been proposed for the K, L, and M intermediate states (Edman et al., 1999; Royant et al., 2000; Sass et al., 2000; Schobert et al., 2002; Lanyi and Schobert, 2002, 2003), proton transfer pathway scenarios were recomputed using each of these structures for the protein environment around retinal. The influence of nearby putative water molecules was also investigated (see Experimental Procedures). One suggested mechanism, the translocation of an hydroxide anion in the direction opposite to proton transfer (Lanyi, 2000), will be the object of a future study and is not included here.

In total, more than 40 different pathways were determined. The most relevant ones are summarized in Table 2. It was found that the pathways and their energy barriers depend little on which crystal structure is used for nonretinal atoms. This is due in part to the flexibility of the retinal environment, which adapts during geometry optimization to a given conformation and protonation state of retinal. More unexpected was that no single mechanism of proton transfer has a significantly lower energy barrier than all the others. The three lowest energy pathways have rate-limiting energy barriers in the 11.5–13.6 kcal/mol range. The 2 kcal/mol difference between these barriers is within the estimated error of the methods used here. The three pathways have different mechanisms, one involving direct proton transfer and the two others involving intermediate proton carriers on either side of the retinal. Their calculated potential energy barriers are close to the experimentally esti-

mated enthalpy barrier of 13 ± 2 kcal/mol for the L-to-M conversion at pH 7 (Ludman et al., 1998). Thus, based on the present calculations, at least three very different mechanisms seem possible for the primary proton transfer step. The events in these pathways are best observed as molecular movies (see web page above) and are described in the next section.

Three Transfer Mechanisms

In path **1a**, the proton is transferred directly from the Schiff base to Asp85 on the Thr89 side of the retinal (green broken arrow in Figure 1C). The energy profile (Figure 3A) for this path exhibits a rate-limiting barrier of 12.4 kcal/mol. This is unexpectedly low, given the large donor-acceptor distance in the CP state (~4 Å). However, the donor-acceptor distance shortens to 2.5 Å at the transition state ($\lambda = 0.36$ in Figure 3A) owing to considerable twisting of the retinal polyene chain and simultaneous displacement of the Asp85 side chain. The barrier increases to 23.4 kcal/mol when preventing motion in the surrounding protein, which indicates that protein flexibility is essential to this mechanism. Direct transfer on the other side of the retinal (magenta broken arrow in Figure 1C) has a very high energy barrier of 27.8 kcal/mol (path **1b**) and is thus excluded.

The mechanism of path **2**, which has been suggested previously (Subramaniam and Henderson, 2000; Edman et al., 2003), is a proton wire through Thr89 (continuous green arrow in Figure 1C). The associated energy barrier is 13.6 kcal/mol (Figure 3B). The Schiff base proton is transferred to the hydroxyl group of Thr89, whose own proton is transferred simultaneously to Asp85. The hydrogen bonds in the CP state are nearly optimally arranged for this (see Figure 2A), such that hardly any motion is required.

In path **3a**, the proton is transferred on the Asp212 side (continuous magenta arrow in Figure 1C), in contrast to paths **1a** and **2**. The pathway begins with a change in the twisting of retinal, going from the CP to the EC state (Figures 2A and 2B) over an 8.2 kcal barrier. Figure 3C shows the energy profile of the subsequent proton transfer steps, which take place with little structural rearrangement. First, the Schiff base proton is transferred to Asp212, with a rate-limiting barrier of 11.5 kcal/mol (at $\lambda = 0.1$) above the initial CP state. The hydrogen-bonding pattern around Asp212 then reorganizes (see molecular movie) to form a proton wire from Asp212 to Asp85 via water w402, with the proton still located on Asp212 at $\lambda = 0.6$. Finally, the protonation switches from Asp212 to Asp85 in a concerted manner via this proton wire. The activation barrier of 4.6 kcal/mol at $\lambda = 0.7$ is not rate limiting.

The other transfer mechanisms have significantly higher rate-limiting barriers. One example is path **4a**, which resembles path **3a** in that the transfer takes place on the Asp212 side via a proton wire through water w402, but without first transferring the proton to Asp212. This requires considerable twisting of the retinal to form the proton wire, resulting in a high barrier of 17.5 kcal/mol. In a variant of this mechanism (path **4b**), the retinal goes through a previously suggested 13,14-*dicis* configuration (Schulten and Tavan, 1978; Gerwert and Siebert, 1986) that is 8.5 kcal/mol higher than the CP state. From there, the path is similar to path **4a** and has a lower rate-limiting barrier of 14.1 kcal/mol relative to the CP state. The other pathway starting from the 13,14-*dicis* configuration, path **3b**, is similar to path **3a** but has a high rate-limiting barrier of 16.7 kcal/mol relative to the CP state. While the EC (paths **1b**, **3a**, and **4a**) or 13,14-*dicis* (paths **3b** and **4b**) conformers are visited transiently along the proton transfer paths, these states have a lifetime of <1 ns during the transition, due to the low proton transfer barrier of ~5 kcal/mol from them. This is further evidence that the EC and 13,14-*dicis* conformations are not the initial pretransfer states accumulating in the photocycle on the microsecond timescale.

Roles of Water w402 and Thr89

Recent studies indicate that water w402, which is in a bridging position between Asp85 and Asp212 (see Figure 1C), is probably present in the L and M states (Lanyi and Schobert 2002, 2003; Tanimoto et al., 2003). Its role in mechanisms **1a** and **2** (i.e., the mechanisms that do not require water w402 to participate in a proton wire) was investigated by recomputing these paths in absence of w402. Removal of water w402 results in energy barriers that are significantly too low. For example, in the case of the direct proton-transfer mechanism, the barrier is reduced from 12.4 kcal/mol (path **1a**) to 6.3 kcal/mol. The reason for this reduction is that the motion of the Asp85 side chain toward the Schiff base is no longer restricted by the hydrogen bond with water w402. The fact that the energy barriers obtained in absence of water w402 are significantly lower than experiment provides additional evidence for the presence of this water molecule in the L and M states.

Paths **1a** and **2** show that the proton can transfer on the side of Thr89, in apparent contradiction with mutational studies that show that the Thr89Val mutant exhibits wild-type rates of retinal deprotonation (Marti et al., 1991). However, recomputing the proton transfer paths in the Thr89Val mutant reveals that direct transfer from the Schiff base to Asp85 (path **5**) has a barrier of 12.3 kcal/mol, close to the value of path **1a** in the wild-type. This confirms that the hydroxyl group of Thr89 is not essential for transfer, but that transfer on the Thr89 side of retinal is still possible in its absence.

Discussion

Figure 4 summarizes the events of the primary transfer. The initial state (CP) has the Schiff base proton oriented toward the cytoplasm. Even though this is apparently the "wrong" direction, transfer from this state is kinetically feasible. The rate-limiting barrier of the lowest energy pathways is in the 11.5–13.6 kcal/mol range, close to the ~13 kcal/mol of the experimentally determined enthalpy of activation (Ludman et al., 1998). Protein flexibility allows a direct transfer (path **1a**). Proton wires allow transfer on the side of Thr89 (path **2**), as well as on the side of Asp212 via an EC conformation (path **3a**), and maybe also via a 13,14-*dicis* conformation (path **4b**). Both sides are still possible in the Thr89Val mutant. It has been foreseen recently that different pathways might

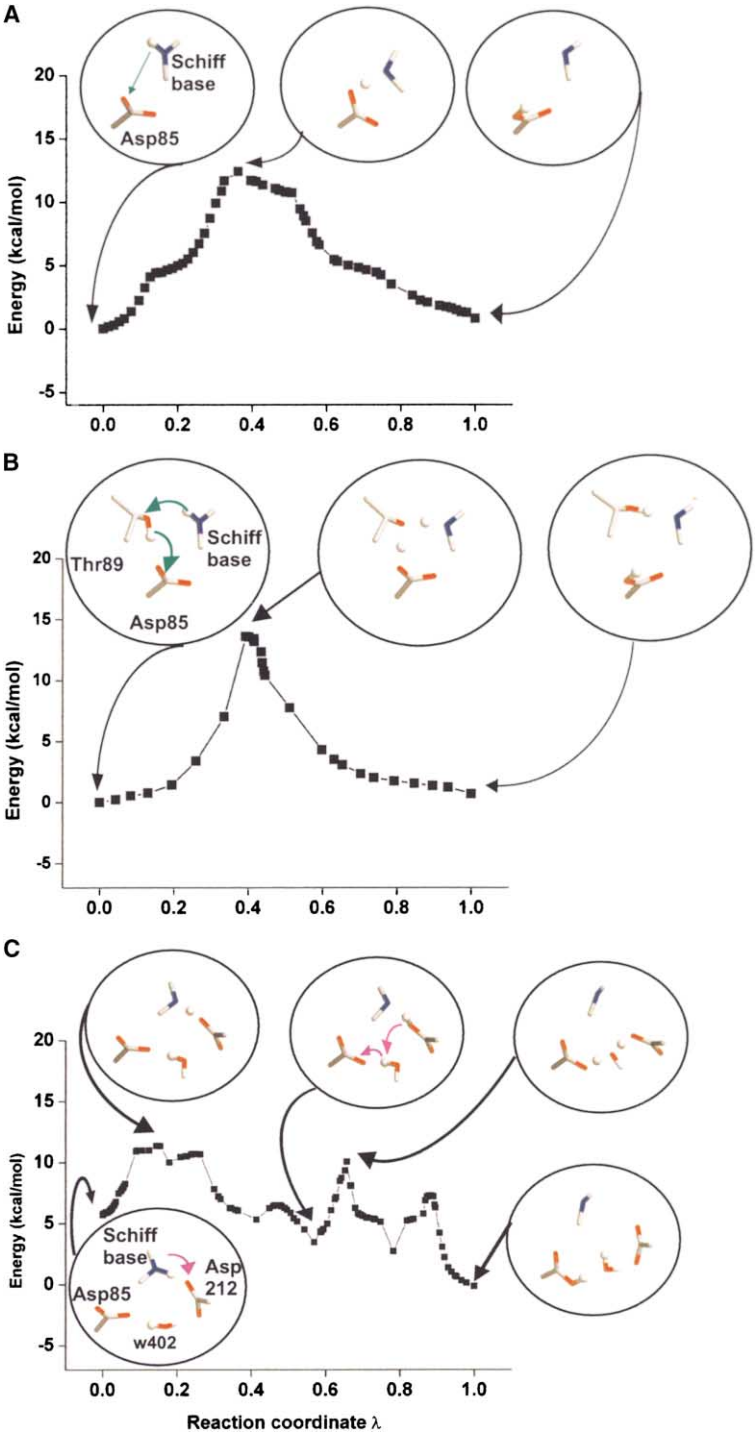

Figure 3. Energy Profiles along Different Proton Transfer Mechanisms

(A) Path **1a**, direct transfer.

(B) Path **2**, proton wire through Thr89.

(C) Path **3a**, transfer to Asp212 followed by proton wire through water w402. λ is the normalized sum along the path of the change in all atomic coordinates (measured as a rms difference) (Fischer et al., 1998). $\lambda = 0$ is the CP state and $\lambda = 1$ is the product P1 (Figures 2A and 2C), except in (C) where $\lambda = 0$ is the EC state and $\lambda = 1$ is P2 (Figures 2B and 2D). Energies are taken relative to the CP state (SCC-DFTB values, see Experimental Procedures). The insets show the transferred protons as small spheres.

contribute to the primary proton transfer (Edman et al., 2003). However, it is surprising that for a transfer over a relatively short distance (4 Å), three very different mechanisms coexist. This may not be fortuitous and could provide a strategy by which the protein renders this crucial step of the photocycle more robust. Under the harsh environmental conditions of halobacteria, some of the transfer pathways might be impeded. Having three different pathway options makes it more likely that one of them will remain functional.

In accordance with several experimental observations, (Réat et al., 1998; Edman et al., 2003) mechanisms **1** and **3** require extensive flexibility in the retinal chain and neighboring residues from helix C (containing Asp85) to bring the donor-acceptor distance within proton transfer range. The usefulness of the QM/MM approach is clear in this case, by allowing the donor and acceptor groups of the quantum region to be carried flexibly by the protein scaffold. Because these proton transfer mechanisms involve the complex interplay of

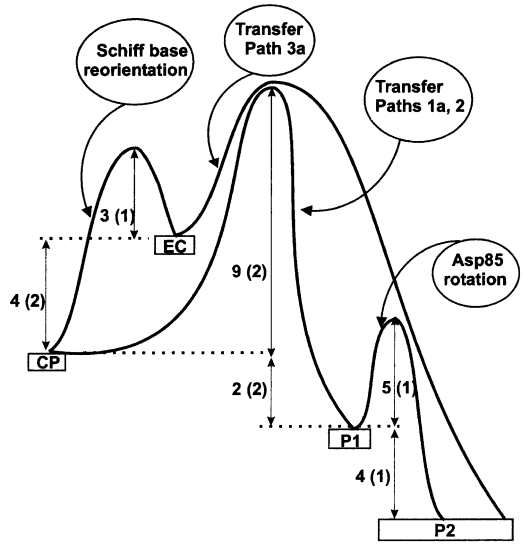

Figure 4. Schematic Energy Profile of Probable Events
Energies are B3LYP/6-31G** values (kcal/mol). Numbers in parentheses are the difference relative to the SCC-DFTB quantum method, giving an error estimate (see Experimental Procedures).

many different degrees of freedom in addition to proton displacement, such as retinal twisting and water rotation, the a priori definition of a suitable reaction coordinate is not practical and the use of an automated method for finding the minimum energy paths proved to be indispensable.

Experimental Procedures

Protein Models

The different orientations of the Schiff base in the available crystal structures (Edman et al., 1999; Royant et al., 2000; Sass et al., 2000; Schobert et al., 2002; Lanyi and Schobert, 2002, 2003) were tested to find which conformations of 13-*cis* retinal are stable in the protonated and deprotonated states. To test the influence of the surrounding protein, paths **1** and **2** were each recomputed with different PDB entries, namely 1QKO (Edman et al., 1999), 1E0P (Royant et al., 2000), and 1CWQ (Sass et al., 2000). Paths **3a** and **4a** were recomputed with entries 1M0K (Schobert et al., 2002) and M0M (Lanyi and Schobert, 2002). Entry 1QKO (Edman et al., 1999) was used for paths **3b**, **4b**, and **5**. Residues 5–231, as well as all buried water molecules were included. Hydrogen atoms were positioned using the HBUILD facility of the CHARMM program (Brooks et al., 1983). Standard protonation was assumed, except for the acidic residues Asp96, Asp115, and Glu204 which were protonated, in accordance with experiment (Metz et al., 1992; Brown et al., 1995). The Thr89Val mutant was modeled by replacing the hydroxyl group of Thr89 by a methyl group.

Water molecules near to retinal are likely to influence the proton transfer mechanism, in particular water molecule w402, which hydrogen bonds to the Schiff base, Asp85, and Asp212 in the bR state (Belrhali et al., 1999; Luecke et al., 1999). In recent, high-resolution structures of the K, L, and early-M intermediates, water w402 is located in positions very similar to that occupied in the bR state (Schobert et al., 2002; Lanyi and Schobert 2002, 2003). FTIR spectroscopy (Tanimoto et al., 2003) also suggests that w402 is present during the primary proton transfer step. Pathways were computed both in the presence and in the absence of water w402.

Potential Energy Function

The protein was partitioned into quantum (QM) and molecular mechanics (MM) parts. The QM region comprised retinal, the side chains of Asp85, Thr89, Asp212, and Lys216 and water w402 (86 QM atoms). The QM/MM interactions have been described (Cui et al., 2001). The link atom approach (Field et al., 1990) was used for the QM/MM boundaries at the C_β-C_γ bond in Lys216 and at the C_α-C_β bond for the other side chains. MM interactions were calculated as described previously (Fischer et al., 1998). The self-consistent-charge density functional tight binding (SCC-DFTB) method (Elstner et al., 1998) was used for the QM region, as it has been shown previously to accurately describe retinal torsion (Zhou et al., 2002), hydrogen-bonded systems (Han et al., 2000), and proton transfer energies (Cui et al., 2001). Because the standard SCC-DFTB underestimates the energy of bond formation between a proton and a neutral nitrogen, this bond strength was reparametrized such that the SCC-DFTB retinal:acetate relative proton affinity is in agreement with B3LYP/6-31G**. The geometry of the end- and saddle points of all pathways were optimized keeping parts of the protein fixed. The mobile region consisted of retinal, nearby water molecules, and one layer of surrounding residues (830 mobile atoms).

To evaluate the dependence of the results on the choice of the quantum method, the energy along the pathways was recalculated without geometry reoptimization using the DFT method B3LYP/6-31G**. The reactant-product energy difference agrees to within 2 kcal/mol. The root-mean-square deviation of the rate-limiting barriers relative to the values obtained using SCC-DFTB is only 2.1 kcal/mol (mean deviation 1.4 kcal/mol) for the transfer pathways below 15 kcal/mol. A similarly small deviation had been found in the case of proton transfer in the enzyme triphosphate isomerase (Cui et al., 2001). Except for Figure 4, all energies given in the article are the geometry-optimized SCC-DFTB values.

Reaction Pathways

Reaction pathways were determined using the Conjugate Peak Refinement (CPR) algorithm (Fischer and Karplus, 1992) as implemented in the TRAVEL module of CHARMM (Brooks et al., 1983). The CPR method has allowed the mechanism of several complex transitions in proteins to be understood (Fischer et al., 1998; Dutzler et al., 2002). The method finds a minimum-energy pathway between predefined reactant and product structures. CPR does not require any a priori definition of a reaction coordinate, which would be difficult for the many different proton transfer mechanisms considered here. Instead, the algorithm starts from an initial guess of the path, which connects the end states and optionally includes initial intermediates. Different proton transfer mechanisms were explored by trying different initial paths. CPR improves a path until it has found a continuous pathway along which all the remaining maxima are first order saddle points of the energy surface. These saddle points give the transition state of the reaction and its rate-limiting energy barriers. Proton tunneling contributions were not considered here, as the experimental kinetic isotope effects have been shown to be rather small for the primary proton transfer step in bR (Brown et al., 2000). Path segments between the saddle points were further refined using the Synchronous Chain Minimization (SCM) algorithm, a "locally updated plane" procedure (Choi and Elber, 1991) implemented in the TRAVEL module.

Acknowledgments

This work was financed by Deutsches Krebsforschungszentrum Heidelberg, the Deutsche Forschungsgemeinschaft, and the Human Frontier Science Program. We thank Prof. András Dér, Dr. Jerôme Baudry, and Mr. Nicolas Calimet for assistance and valuable discussions. We are grateful to Prof. Janos K. Lanyi for providing the crystal structures 1M0K and 1M0M prior to their release in the Protein Data Bank.

Received: January 13, 2004
Revised: March 17, 2004
Accepted: April 6, 2004
Published: July 13, 2004

References

Belrhali, H., Nollert, P., Royant, A., Menzel, C., Rosenbusch, J.P., Landau, E.M., and Pebay, E.P. (1999). Protein, lipid and water organi-

zation in bacteriorhodopsin crystals: a molecular view of the purple membrane at 1.9 Å resolution. Structure *7*, 909–917.

Brooks, B.R., Bruccoleri, R.E., Olafson, B.D., States, D.J., Swaminathan, S., and Karplus, M. (1983). CHARMM: a program for macromolecular energy minimization and dynamics calculations. J. Comput. Chem. *4*, 187–217.

Brown, L.S., Sasali, J., Kandori, H., Maeda, A., Needleman, R., and Lanyi, J.K. (1995). Glutamic acid 204 is the terminal release group at the EC surface of bacteriorhodopsin. J. Biol. Chem. *270*, 27122–27126.

Brown, L.S., Needleman, R., and Lanyi, J.K. (2000). Origins of the deuterium kinetic isotope effects on the proton transfers of the bacteriorhodopsin photocycle. Biochemistry *39*, 938–945.

Choi, C., and Elber, R. (1991). Reaction path study of helix formation in tetrapeptides: effect of side chains. J. Chem. Phys. *94*, 751–760.

Cui, Q., Elstner, M., Kaxiras, E., Frauenheim, T., and Karplus, M. (2001). A QM/MM implementation of the self-consistent charge density functional tight binding (SCC-DFTB) method. J. Phys. Chem. B *105*, 569–585.

Dutzler, R., Schirmer, T., Karplus, M., and Fischer, S. (2002). Translocation mechanism of long sugar chains across the maltoporin membrane channel. Structure *10*, 1273–1284.

Edman, K., Nollert, P., Royant, A., Belrhali, H., Peyroula, E.P., Hajdu, J., Neutze, R., and Landau, E.M. (1999). High-resolution X-ray structure of an early intermediate in the bacteriorhodopsin photocycle. Nature *401*, 822–826.

Edman, K., Royant, A., Larsson, G., Jacobson, F., Taylor, T., van der Spoel, D., Landau, E.M., Pebay-Peyroula, E., and Neutze, R. (2003). Deformation of helix C in the low-temperature L-intermediate of bacteriorhodopsin. J. Biol. Chem. *279*, 2147–2158.

Elstner, M., Porezag, D., Jungnickel, G., Elsner, J., Haugk, M., Frauenheim, T., Suhai, S., and Seifert, G. (1998). Self-consistent-charge density-functional tight-binding method for simulations of complex materials properties. Phys. Rev. B *58*, 7260–7268.

Field, M.J., Bash, P.A., and Karplus, M. (1990). A combined quantum mechanical and molecular mechanical potential for molecular dynamics simulations. J. Comput. Chem. *11*, 700–733.

Fischer, S., and Karplus, M. (1992). Conjugate Peak Refinement: an algorithm for finding reaction paths and accurate transition states in systems with many degrees of freedom. Chem. Phys. Lett. *194*, 252–261.

Fischer, S., Verma, C.S., and Hubbard, R.E. (1998). Rotation of structural water inside a protein: calculation of the rate and vibrational entropy of activation. J. Phys. Chem. B *102*, 1797–1805.

Gerwert, K., and Siebert, F. (1986). Evidence for light-induced 13-cis, 14-s-cis isomerization in bacteriorhodopsin obtained by FTIR difference spectroscopy using isotopically labelled retinals. EMBO J. *4*, 805–811.

Griffiths, J.M., Bennet, A.E., Engelhard, M., Siebert, F., Raap, J., Lugtemburg, J., Herzfeld, J., and Griffin, R.G. (2000). Structural investigation of the active site in bacteriorhodopsin: geometric constraints on the roles of Asp-85 and Asp-212 in the proton-pumping mechanism from solid state NMR. Biochemistry *39*, 362–371.

Han, W.G., Elstner, M., Jalkanen, K.J., Frauenheim, T., and Suhai, S. (2000). Hybrid SCC-DFTB/Molecular Mechanical studies of H-bonded systems and of n-acetyl-(L-Ala)$_n$ N'-methylamide helices in water solution. Int. J. Quantum Chem. *78*, 459–479.

Hu, J.G., Sun, B.Q., Bizounok, M., Hatcher, M.E., Lansing, J.C., Raap, J., Verdegen, P.J.E., Lugtemburg, J., Griffin, R.G., and Herzfeld, J. (1998). Early and late M photointermediates in the bacteriorhodopsin photocycle: a solid-state NMR study. Biochemistry *37*, 8088–8096.

Kandori, H., Yamazaki, Y., Shichida, Y., Raap, J., Lugtemburg, J., Belenky, M., and Herzfeld, J. (2001). Tight Asp-85-Thr89 association during the pump switch of bacteriorhodopsin. Proc. Natl. Acad. Sci. USA *98*, 1571–1576.

Lansing, J.C., Hohwy, M., Jaroniec, C.P., Creemers, A.F.L., Lugtemburg, J., Herzfeld, J., and Griffin, R.G. (2002). Chromophore distortions in the bacteriorhodopsin photocycle: evolution of the H-C14–C15-H dihedral angle as measured by solid-state NMR. Biophys. J. *41*, 431–438.

Lanyi, J.K. (2000). Molecular mechanism of ion transport in bacteriorhodopsin: insights from crystallographic, spectroscopic, kinetic and mutational studies. J. Phys. Chem. B *104*, 11441–11448.

Lanyi, J.K., and Schobert, B. (2002). Crystallographic structure of the retinal and the protein after deprotonation of the Schiff base: the switch in the bacteriorhodopsin photocycle. J. Mol. Biol. *321*, 727–737.

Lanyi, J.K., and Schobert, B. (2003). Mechanism of the proton transport in bacteriorhodopsin from crystallographic structures of the K, L, M_1, M_2, and M_2' intermediates of the photocycle. J. Mol. Biol. *328*, 439–450.

Ludman, K., Gergely, C., and Váró, G. (1998). Kinetic and thermodynamic study of the bacteriorhodopsin photocycle over a wide pH range. Biophys. J. *75*, 3110–3119.

Luecke, H., Schobert, B., Richter, H.T., Cartailler, J.P., and Lanyi, J.K. (1999). Structure of bacteriorhodopsin at 1.55 Å resolution. J. Mol. Biol. *291*, 899–911.

Marti, T., Otto, H., Mogi, T., Rösselet, S.J., Heyn, M.P., and Khorana, H.G. (1991). Bacteriorhodopsin mutants containing single substitutions of serine or theronine residues are all active in proton translocation. J. Biol. Chem. *266*, 6919–6927.

Metz, G., Siebert, F., and Engelhard, M. (1992). Asp^{85} is the only internal aspartic acid that gets protonated in the M intermediate and the purple-to-blue transition of bacteriorhodopsin. A solid-state ^{13}C CP-MAS NMR investigation. FEBS Lett. *303*, 237–241.

Neutze, R., Pebay-Peyroula, E., Edman, K., Royant, A., Navarro, J., and Landau, E.M. (2002). Bacteriorhodopsin: a high-resolution structural view of vectorial proton transport. Biochim. Biophys. Acta *1565*, 144–167.

Réat, V., Patzelt, H., Ferrand, M., Pfister, C., Oesterhelt, D., and Zaccai, G. (1998). Dynamics of different functional parts of bacteriorhodopsin: H-H^2 labelling and neutron scattering. Proc. Natl. Acad. Sci. USA *95*, 4970–4975.

Royant, A., Edman, K., Ursby, T., Peyroula, E.P., Landau, E.M., and Neutze, R. (2000). Helix deformation is coupled to vectorial proton transport in the photocycle of bacteriorhodopsin. Nature *406*, 645–648.

Sass, H., Büldt, G., Gessenich, R., Hehn, D., Neff, D., Schlesinger, R., Berendzen, J., and Ormos, P. (2000). Structural alterations for proton transport translocation in the M state of wild-type bacteriorhodopsin. Nature *406*, 649–652.

Schobert, B., Cupp-Vickery, J., Hornak, V., Smith, S.O., and Lanyi, J.K. (2002). Crystallographic structure of the K intermediate of bacteriorhodopsin: conservation of free energy after photoisomerization of the retinal. J. Mol. Biol. *321*, 715–716.

Schulten, K., and Tavan, P. (1978). A mechanism for the light-driven proton pump of *Halobacterium Salinarium*. Nature *272*, 85–86.

Subramaniam, S., and Henderson, R. (2000). Molecular mechanism of vectorial proton translocation by bacteriorhodopsin. Nature *406*, 653–657.

Subramaniam, S., Lindahl, M., Bullough, P., Faruki, A.R., Tittor, J., Oesterhelt, D., Brown, L., Lanyi, J.K., and Henderson, R. (1999). Protein conformational changes in the bacteriorhodopsin photocycle. J. Mol. Biol. *287*, 145–146.

Tanimoto, T., Furutani, Y., and Kandori, H. (2003). Structural changes of water in the Schiff base region of bacteriorhodopsin: proposal of a hydration switch model. Biochemistry *42*, 2300–2306.

Zhou, H., Tajkhorshid, T., Suhai, S., and Elstner, M. (2002). Performance of the AM1, PM3, and SCC-DFTB methods in the study of conjugated Schiff base molecules. Chem. Phys. Lett. *277*, 91–103.